Journal of Power Sources 182 (2008) 482–488

Contents lists available at ScienceDirect

Journal of Power Sources

journal homepage: www.elsevier.com/locate/jpowsour

Characterization and electrochemical performances of $Ba_{2-x}Sr_xFeO_{4+\delta}$ as a novel cathode material for intermediate-temperature solid oxide fuel cells

Chao Jin, Jiang Liu*, Yaohui Zhang, Jing Sui, Weimin Guo

School of Chemistry and Chemical Engineering, South China University of Technology, 381 Wushan Road, Guangzhou 510641, PR China

ARTICLE INFO

Article history:
Received 2 March 2008
Received in revised form 17 April 2008
Accepted 18 April 2008
Available online 29 April 2008

Keywords:
Cathode materials
$A_2BO_{4+\delta}$ compounds
Thermogravimetric analysis
Electrochemical properties
Solid oxide fuel cells

ABSTRACT

Novel cathode materials, $Ba_{2-x}Sr_xFeO_{4+\delta}$ ($x = 0.5, 0.6, 0.7, 0.8, 1.0$), for intermediate-temperature solid oxide fuel cells on a samaria-doped ceria (SDC) electrolyte were prepared by the glycine–nitrate route and characterized by X-ray diffraction (XRD), Fourier-transform infrared (FTIR) spectroscopy, scanning electron microscopy (SEM), thermogravimetric (TG) analysis, electrochemical impedance spectroscopy and steady-state polarization measurement. SEM results showed that the electrode formed a good contact with the SDC electrolyte after sintering at 1000 °C for 2 h. The value of δ in $Ba_{1.0}Sr_{1.0}FeO_{4+\delta}$ materials was calculated from the TG results. The electrochemical impedance spectra revealed that $Ba_{2-x}Sr_xFeO_{4+\delta}$ had a better electrochemical performance than that of Ln_2NiO_4 (Ln = La, Pr, Nd, Sm). In the $Ba_{2-x}Sr_xFeO_{4+\delta}$ ($x = 0.5$, 0.6, 0.7, 0.8, 1.0) family, the composition $Ba_{1.0}Sr_{1.0}FeO_{4+\delta}$ exhibited the best electrochemical activity for oxygen reduction. The polarization resistance of $Ba_{1.0}Sr_{1.0}FeO_{4+\delta}$ on SDC electrolyte was 1.11 $\Omega\,cm^2$ at 700 °C, which was less than half that reported for Ln_2NiO_4 at the same temperature.

1. Introduction

Solid oxide fuel cells (SOFCs) have been targeted for both mobile and stationary power-generation systems. However, one of the most important handicaps for their commercialization is the high fabrication and operating costs, which result from their high operating temperatures (900–1000 °C) [1]. Thus, many efforts have been focused on reducing the SOFC operating temperature without decreasing the cell efficiency. Generally, ohmic resistance from the electrolyte and polarization from the electrodes make up the main losses of a SOFC. It is reckoned that polarization at the anode is negligible compared to that of the cathode, at least in the case of hydrogen SOFCs [2]. So, a better SOFC performance at lower temperatures can be realized by improving the performance of the cathode. Mixed ionic–electronic conducting oxides are promising cathode materials since their cathode kinetic reaction is improved by replacing the triple-phase-boundary (TPB) zone (electrolyte–cathode–air) with a double inter-phase (cathode–air) at intermediate temperatures. Mixed conductors are already one of the best choices for reducing the operating temperature of SOFCs and have attracted a lot of attention [3,4].

Perovskite-type oxides with ABO_3 structure, such as $La_{1-x}Sr_xCoO_3$ (LSC), are good mixed conductors and have been tested as cathodes for SOFCs. However, these LSC cathodes have thermomechanical stability problems due to their significantly large thermal expansion coefficients. Previously, many studies have shown that materials with perovskite-related K_2NiF_4-type (or A_2BO_4) structure, such as Ln_2NiO_4, are mixed ionic–electronic conductors and exhibit good electronic conductivity (due to the metal mixed valency), ionic-transport properties (due to the oxygen overstoichiometry), electrocatalysis (due to oxygen reduction) and thermal expansion properties [5–8]. Therefore, $A_2BO_{4+\delta}$ materials have been mainly used as oxygen separators, oxygen sensors and low-temperature superconductors, for example [9]. At present, these oxides are being extensively re-examined concerning their possible use as cathode materials for intermediate-temperature SOFCs (IT-SOFCs). Compared to the perovskite-structured cathodes commonly used for SOFCs, K_2NiF_4-type materials possess better thermal stability and smaller thermal expansion coefficients ($10.5–14.2 \times 10^{-6}\,K^{-1}$) [7,10,11] that match better with those of the commonly used electrolytes YSZ, GDC and SDC. Taking $Ln_2NiO_{4+\delta}$ (Ln = Pr, Nd) as examples, their surface oxygen-exchange coefficients and oxide-ion diffusivities are much higher than those of $La_{1-x}Sr_xFe_{1-y}Co_yO_{3-\delta}$ [12,13].

Among K_2NiF_4-type A_2BO_4 compounds for potential use as SOFC cathodes, $Ln_2NiO_{4+\delta}$-based materials, where Ln is usually some rare-earth element, such as La, Pr, Nd, or Sm, containing excess oxygen, have attracted the most attention [14–19]. Another group of compounds that adopts the same structure and also contains excess oxygen is the phase $La_xSr_{2-x}FeO_{4+\delta}$. Jennings and Skinner

* Corresponding author. Tel.: +86 20 2223 6168; fax: +86 20 2223 6168.
E-mail address: jiangliu@scut.edu.cn (J. Liu).

0378-7753/$ – see front matter © 2008 Elsevier B.V. All rights reserved.
doi:10.1016/j.jpowsour.2008.04.044

suggested these materials as possible cathodes for SOFCs through a study of their thermal stability and conduction properties [20]. To the best of the authors' knowledge, there are few papers (e.g. [21]) in which rare-earth elements are completely replaced with alkaline-earth metals in the A site of the $A_2BO_{4+\delta}$ materials and their cathode properties are investigated. It has been reported that doping with Sr improves the p-type electrical conductivity of $La_{2-x}Sr_xNiO_4$ nickelates [22], and different kinds of oxygen defects can be formed, depending on the Sr doping concentration [23]. It is generally believed that these oxygen defects offer the possibility of rapid oxygen transport through the ceramic material. In the present study, materials in the $Ba_{2-x}Sr_xFeO_{4+\delta}$ series have been synthesized and characterized. The results of the investigation indicate that better cathodic properties can be obtained by completely replacing rare-earth elements with alkaline-earth metals.

2. Experimental

2.1. Preparation and measurement of materials

$Ba_{2-x}Sr_xFeO_{4+\delta}$ (x = 0.5, 0.6, 0.7, 0.8, 1.0) materials were synthesized via the glycine–nitrate route [24]. Stoichiometric amounts of analytical-grade $Ba(NO_3)_2$, $Sr(NO_3)_2$ and $Fe(NO_3)_3{\cdot}9H_2O$ were dissolved and mixed in pure water. Glycine was then added to the mixture in the molar ratio of 2:1 with respect to the total number of metal ions. The solution was heated to ignition on a hot plate to obtain a powder precursor. The precursor was calcined in air at 1000 °C for 8 h. For convenience, the obtained materials were called BSF1010 for $Ba_{1.0}Sr_{1.0}FeO_{4+\delta}$ (or $BaSrFeO_{4+\delta}$), BSF1208 for $Ba_{1.2}Sr_{0.8}FeO_{4+\delta}$, and so on. $Sm_{0.2}Ce_{0.8}O_{1.9}$ (SDC) powder was prepared using a citric–nitrate process and calcining at 800 °C for 2 h [25]. The powder was then pressed into pellets and sintered at 1400 °C for 4 h.

The crystal structure of the powders was examined by X-ray diffraction (XRD) using a Bede D^1 X-ray diffractometer (Bede Scientific Ltd., UK) with Cu Kα radiation operating at 40 kV, 45 mA; λ = 0.15418 nm. The diffraction angle was varied from 20° to 80° with a step of 0.02° and a scan rate of 1.2° min^{-1}. Fourier-transform infrared (FTIR) spectroscopy of the $Ba_{2-x}Sr_xFeO_{4+\delta}$ (x = 0.5, 0.6, 0.7, 0.8, 1.0) materials sintered at 1000°C for 8 h in air was performed on a PerkinElmer 1730 spectrophotometer in the mid-IR range from 4000 to 400 cm^{-1} and with a resolution of 4 cm^{-1} using KBr pellets as standards. The morphology of the synthesized powders and the microstructure of the sintered electrodes were examined with a Hitachi S-3000N scanning electron microscope. The oxygen content (δ) of these materials was determined by TG analysis using an INC Q600 SDT analyzer.

2.2. Fabrication and measurement of half-cells

A typical three-electrode method was used to perform electrochemical characterization of the $Ba_{2-x}Sr_xFeO_{4+\delta}$ cathodes on an SDC electrolyte in air. Each sample of $Ba_{2-x}Sr_xFeO_{4+\delta}$ powder was mixed with an organic binder (ethyl cellulose, α-terpineol) in a weight ratio of 1:1 to form a cathodic ink, which was subsequently painted on one side of an SDC pellet to form a working electrode (WE) with an effective area of 0.20 cm^2. After the cathode was sintered at 1000 °C for 2 h, Ag paste was painted on the other side of the SDC pellet, symmetrically opposite to the cathode, as the counter electrode (CE). A silver reference electrode (RE) was attached to the same side of the WE by painting Ag paste on an uncoated region at the edge of the substrate. The distance between the edges of the RE and WE was about 3 mm. An Ag grid was printed on the surface of the cathode to serve as a current collector. Before testing, the half-cell was heated at 250 °C for 2 h to remove organic solvents and binders. Electrochemical impedance spectroscopy (EIS) and steady-state polarization measurement of the half-cells were carried out with an AUTOLAB PGStat30 electrochemical analyzer. For the EIS measurement, the frequency ranged from 0.1 to 100 kHz and the AC amplitude was 5 mV. For the steady-state polarization measurement of the half-cells, IR compensation was carried out with interrupt method to take out the Ohm polarization.

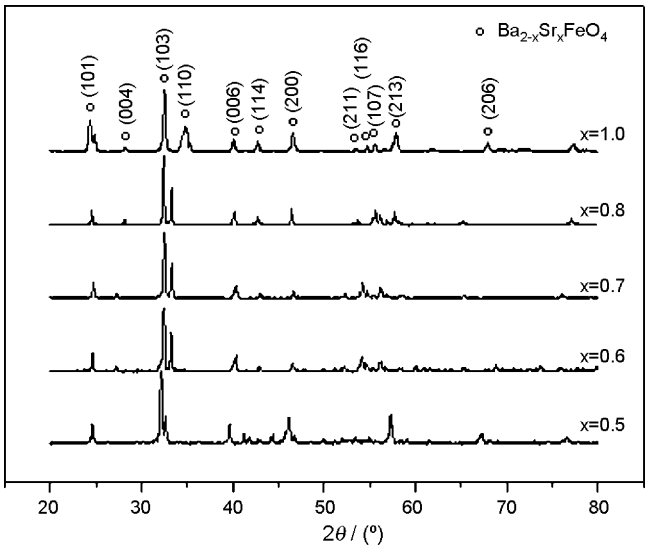

Fig. 1. XRD patterns of $Ba_{2-x}Sr_xFeO_{4+\delta}$ (x = 0.5, 0.6, 0.7, 0.8, 1.0) materials sintered at 1000 °C for 8 h in air.

3. Results and discussion

3.1. Characterization of powders

Fig. 1 shows the XRD patterns of prepared $Ba_{2-x}Sr_xFeO_{4+\delta}$ (x = 0.5, 0.6, 0.7, 0.8, 1.0) powders after calcining in air at 1000 °C for 8 h. There were peaks other than those of the $A_2BO_{4+\delta}$ structure for the specimens with x = 0.5, 0.6, whereas the samples with x = 0.7, 0.8, 1.0 basically crystallized in a single phase with $A_2BO_{4+\delta}$ structure, and no impurities were found [26,27]. It is well known that reaction between the electrode and electrolyte is undesirable for the long-term stability of a SOFC. The reactivity of BSF1010 with the SDC electrolyte was further studied by mixing BSF1010 and SDC powders with a 1:1 weight ratio, and then sintering at 1000 °C for 2 h. Fig. 2 shows the XRD patterns of BSF1010, SDC and this BSF1010–SDC mixture. Fig. 2(c) clearly shows that the main peaks of BSF1010 and SDC were present, except for the shifting of some peaks of BSF1010 at about 40°, indicating that BSF1010 was chemical compatibility with the SDC electrolyte at certain extent.

Fig. 3 shows the FTIR spectra of the $Ba_{2-x}Sr_xFeO_{4+\delta}$ (x = 0.5, 0.6, 0.7, 0.8, 1.0) materials sintered at 1000 °C for 8 h in air. In the range of the figure, the absorption peak at about 500 cm^{-1} is assigned to the retractile vibration of the $A–O_{(II)}–B$ bond in the A_2BO_4 compound, which is a characteristic absorption of A_2BO_4 materials in the FTIR spectrum [27,28]. The FTIR results also showed that increasing the Sr doping content could promote the formation of a single A_2BO_4-structural phase for $Ba_{2-x}Sr_xFeO_{4+\delta}$ materials.

3.2. TG and differential scanning calorimetry (DSC) analyses

The crystal structure of these $A_2BO_{4+\delta}$ materials can be described as stacked perovskite (ABO_3) layers alternating with

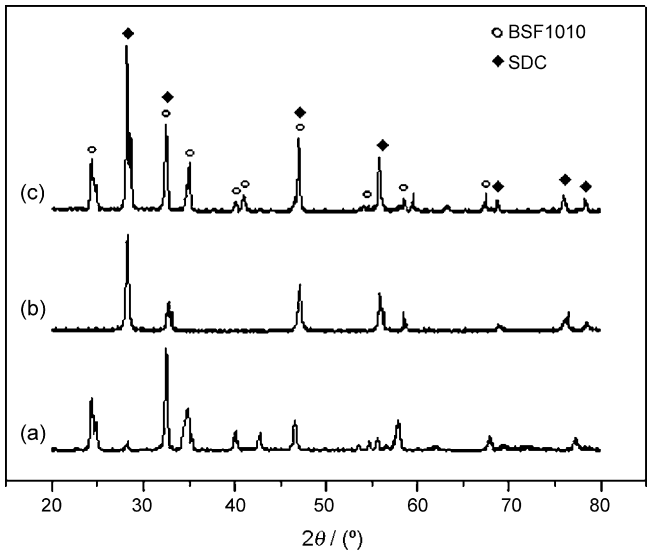

Fig. 2. XRD patterns of (a) BSF1010 final powder after calcining at 1000 °C for 8 h; (b) SDC final powder; (c) BSF1010–SDC mixture after sintering at 1000 °C for 2 h.

rock-salt (AO) layers along the *c* direction. Because of the difference in A–O and B–O bond lengths, there is stress in the $A_2BO_{4+\delta}$ structure. In order to eliminate this stress and maintain the structural stability, there are always interstitial oxygens between the ABO_3 perovskite layers and the AO rock-salt layers [29]. In the $A_2BO_{4+\delta}$ materials, oxygen transport occurs via a complex mechanism combining interstitial migration in the rock-salt layers and vacancy migration in the perovskite planes [30,31]. The contribution of the interstitial mechanism appears to be more important than the vacancy migration mechanism, since a higher oxygen content, which usually has a positive effect on their ionic conductivity, can be achieved in these materials [13,32]. So, the more oxygen overstoichiometry (δ) is achieved in these materials, the better their electrochemical properties can be expected to be.

The TG and DSC curves under N_2 flow of BSF1010 from 28 to 1000 °C, are shown in Fig. 4. In the heating stage there is a weight loss in the temperature range 340–400 °C. This weight loss was identified as the release of excess oxygen (δ) [30]. In this manner,

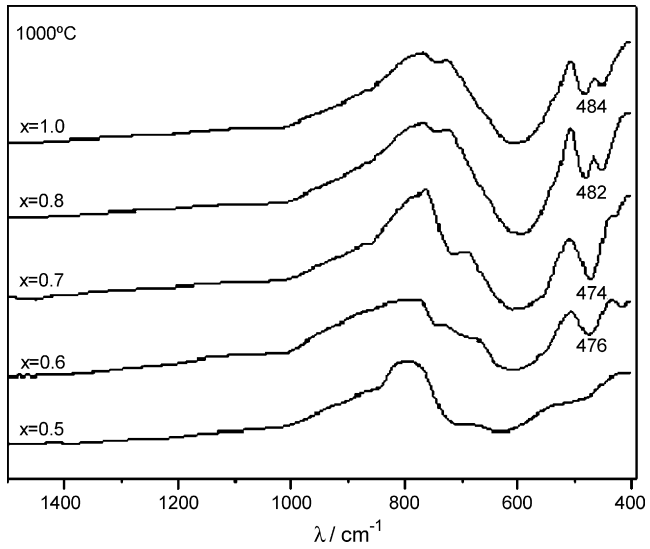

Fig. 3. FTIR spectra of $Ba_{2-x}Sr_xFeO_{4+\delta}$ (x = 0.5, 0.6, 0.7, 0.8, 1.0) materials sintered at 1000 °C for 8 h in air.

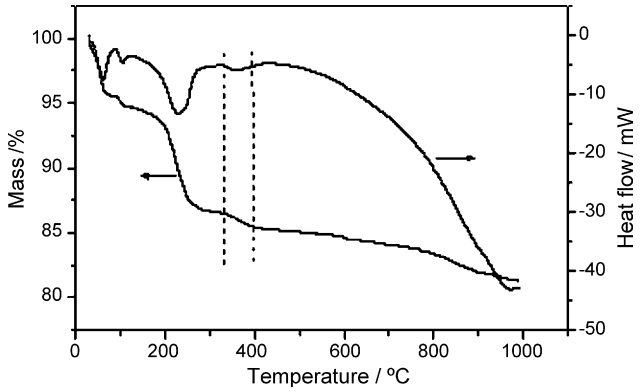

Fig. 4. TG and DSC traces of a BSF1010 sample under N_2 flow in the temperature range 28–1000 °C, at a heating rate of 10 °C min^{-1}.

the oxygen overstoichiometry (δ) content can be easily obtained from the TG analysis, according to the following equation:

$$\frac{\omega\% m}{16} = \frac{m}{M}\delta \quad (1)$$

where ω% is the weight loss of oxygen overstoichiometry (δ), m is the mass of BSF1010, and M is the molar mass of BSF1010. Based on the TG analysis and Eq. (1), the value of δ is calculated to be 0.24 in the BSF1010 sample, larger than the values reported for $La_2Ni_{0.6}Cu_{0.4}O_{4+\delta}$ (0.16) [33] and $La_2NiO_{4+\delta}$ (0.148) [34]. Hereafter, the notation 'BSF1010' indicates the composition $Ba_{1.0}Sr_{1.0}FeO_{4.24}$.

3.3. Sintering effect

In order to investigate the effect of sintering temperature on the properties of a $Ba_{2-x}Sr_xFeO_{4+\delta}$ cathode, different sintering conditions were studied. Fig. 5 shows the impedance spectroscopy of a BSF1010 cathode sintered at 900, 1000, 1100, and 1200 °C. The test was carried out at 700 °C in air on an SDC electrolyte. The intercepts of the impedance arcs on the real axis at high frequencies correspond to the resistance of the electrolyte and lead wires (R_s), while the overall size of the arcs is attributed to cathode polarization resistance (R_p). From the impedance spectra, it was seen that R_p was relatively large when the sintering temperature was low (900 °C). When the sintering

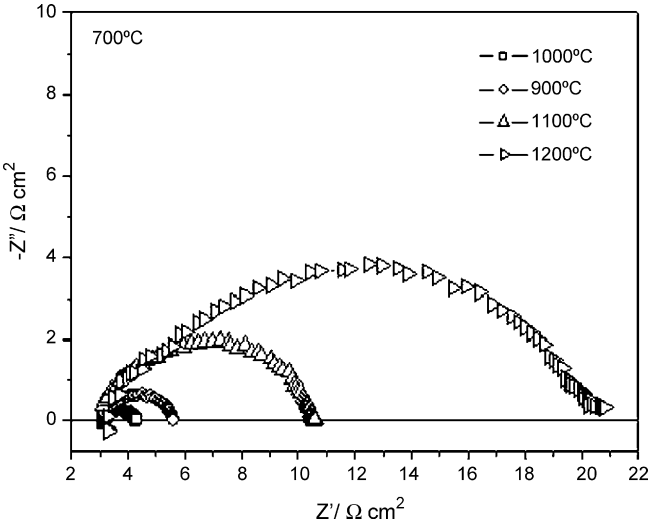

Fig. 5. Impedance spectra of a BSF1010 cathode sintered at different temperatures for 2 h and then measured at 700 °C in air.

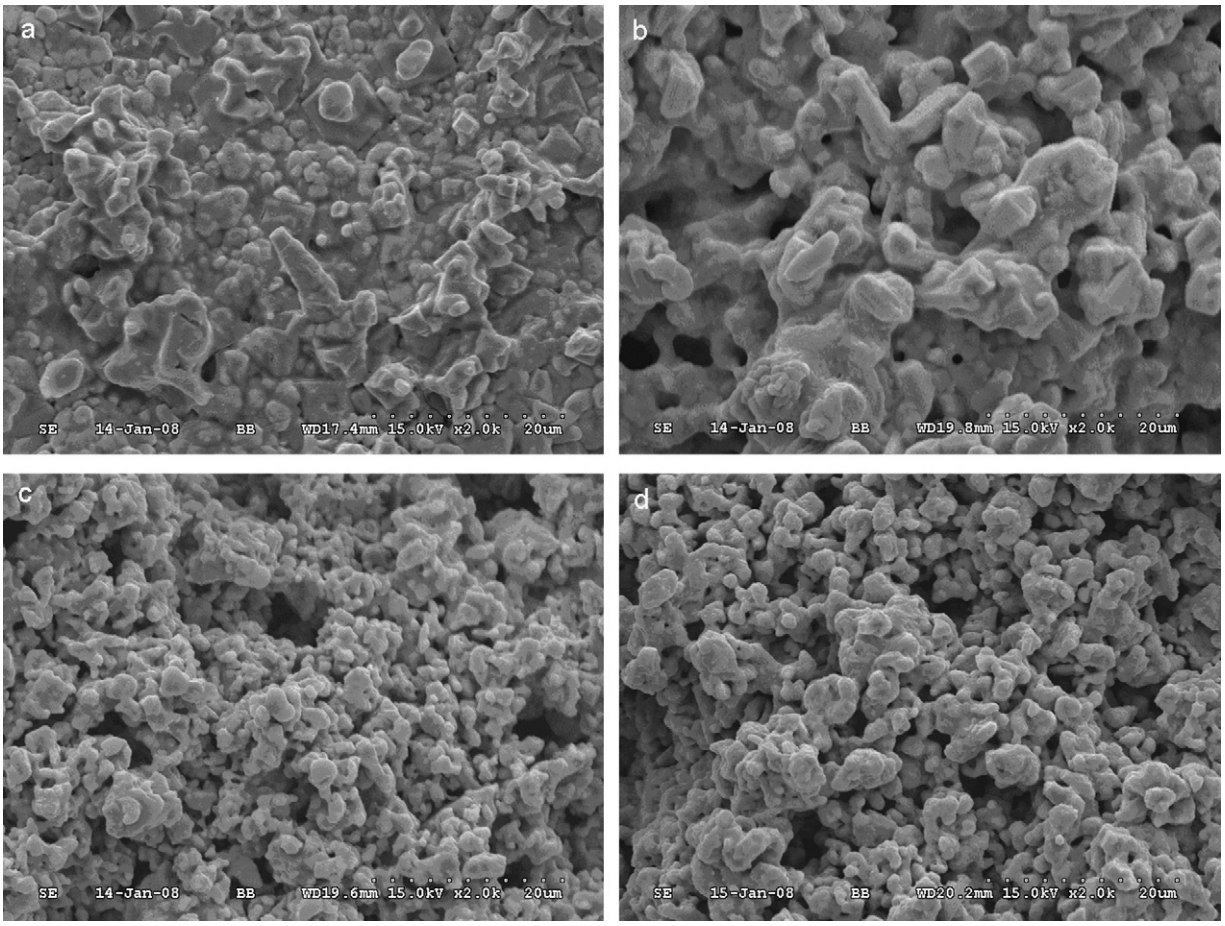

Fig. 6. SEM images of the surfaces of (a) a BSF1010 electrode sintered at 1200 °C; (b) 1100 °C; (c) 1000 °C; (d) 900 °C.

temperature was 1000 °C, R_p decreased to its lowest value. R_p increased again when the sintering temperatures were 1100 and 1200 °C.

It is well known that the sintering temperature has a dramatic effect on the electrode microstructure, which in turn influences the electrode properties. Therefore, the microstructure of the sintered electrode at different temperatures was further studied. Fig. 6 shows SEM images of the surface of BSF1010 electrodes sintered at 1200, 1100, 1000 and 900 °C, respectively, for 2 h. It can be seen that an over-sintering phenomenon appears for the electrode sintered above 1100 °C; in particular, there is almost no porosity for the sample sintered at 1200 °C. Sintering at 1000 °C results in a structure with moderate porosity (Fig. 6(c)). When the electrode is sintered at 900 °C, however, the BSF1010 particles form poor contacts with each other.

Fig. 7 shows cross-sectional images of the interface of the electrolyte and the electrode co-sintered at different temperatures. The electrode sintered at 900 °C (Fig. 7(d)) shows poorer contact with the SDC electrolyte in comparison with electrodes sintered at higher temperatures. Although Fig. 7(a) and (b) show better contact between the BSF1010 cathode and the SDC electrolyte, the higher sintering temperature brings about the over-sintering phenomenon. In general, a high sintering temperature increases the grain size of the electrode and thus decreases the electrode porosity and TPB length, resulting in a high polarization resistance [35]. It can be concluded from the above discussion that 1000 °C for 2 h is the best sintering condition for the as-made BSF1010 cathode on an SDC electrolyte.

3.4. Electrochemical performance

Electrochemical impedance spectroscopy under open-circuit-potential conditions was performed for a $Ba_{2-x}Sr_xFeO_{4+\delta}$ cathode on an SDC electrolyte at 700 °C and the results are shown in Fig. 8. From the impedance spectra, it can be seen that the R_p of the $Ba_{2-x}Sr_xFeO_{4+\delta}$ cathode changes from 1.11 Ω cm^2 for BSF1010 to 1.93 Ω cm^2 for BSF1505 at 700 °C in air. The R_p of BSF1010 is only 1.11 Ω cm^2, which is less than half the values reported for $SmSrCoO_4$ (2.30 Ω cm^2), $Sm_{1.0}Sr_{1.0}NiO_4$ (3.06 Ω cm^2), and $La_{1.6}Sr_{0.4}NiO_4$ (2.93 Ω cm^2) electrode materials at the same temperature [11,19,36]. This may be attributed to the increasing number of interstitial oxygen atoms caused by replacing the smaller radius Ln^{3+} (Ln = La, Pr, Nd, Sm) with a bigger-radius Ba^{2+} in the A site. As we know, the oxygen overstoichiometry (δ) in these materials plays an important role in improving their electrode properties.

In order to clearly clarify the electrochemical process, the equivalent circuits and fitting results of these cathodes are presented in Fig. 9 and Table 1, respectively. Under open-circuit-potential conditions, the impedance spectrum can be decomposed into a resistance and two capacitive arcs. Here, R_s represents the intercept value of the impedance spectrum at the high-frequency side with the real axis, which corresponds to the resistance of the electrolyte and lead wires; and (R_1, Q_1) and (R_2, Q_2) correspond to the high- and low-frequency arcs, respectively. The high-frequency arc (R_1, Q_1) is interpreted as oxygen ion transfer from the electrode to the oxygen-ion vacancies of the cathode or to the grain-boundary resistance of the SDC component. The low-frequency arc (R_2, Q_2) reflects the oxy-

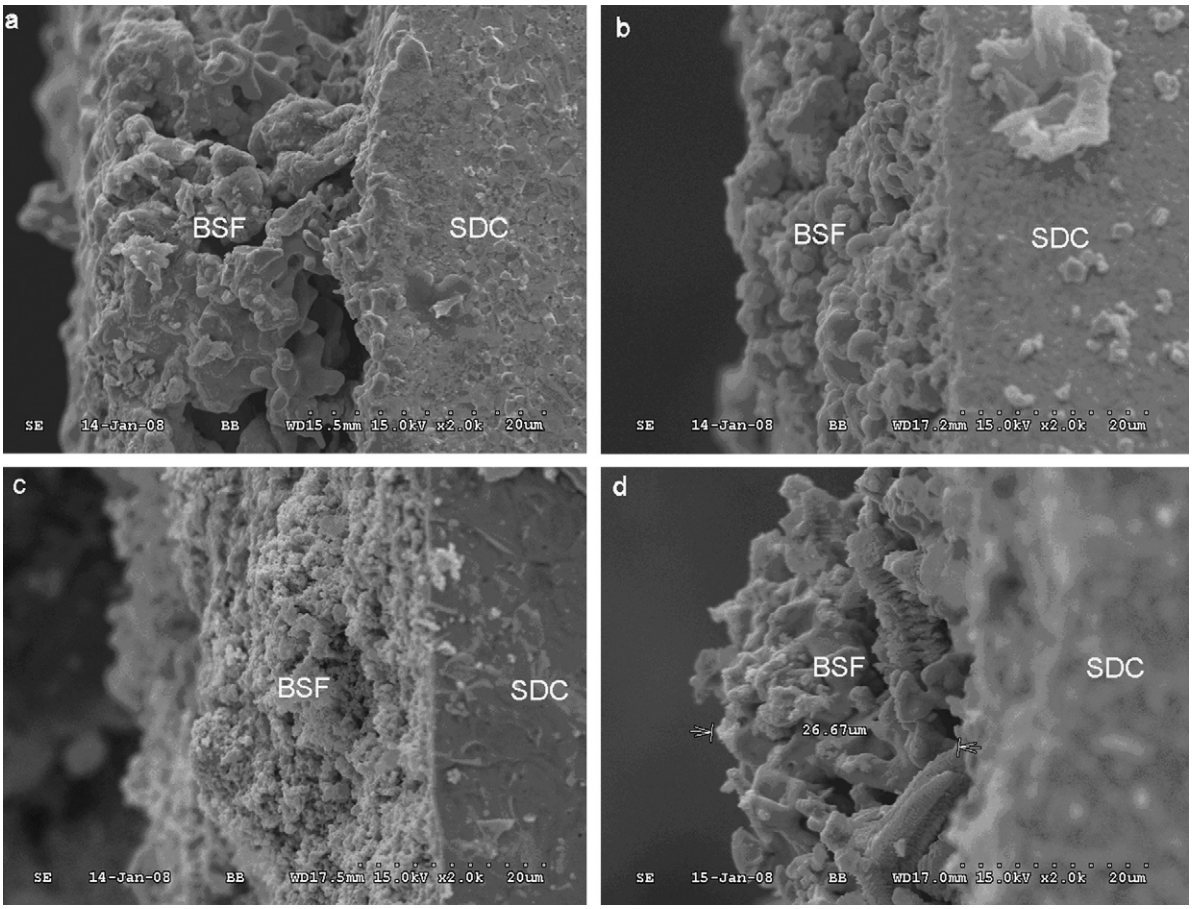

Fig. 7. SEM pictures of the cross-sections of a BSF1010 electrode sintered at (a) 1200 °C; (b) 1100 °C; (c) 1000 °C; (d) 900 °C.

Table 1
Experimental data and fitting parameters extracted from EIS results at 700 °C

	Experimental data		Fitted values of the different parameters					
	R_s	R_p	R_s	R_1	Q_1	R_2	Q_2	R_1+R_2
BSF1010	3.182	1.115	3.137	0.6585	0.0063	0.4992	0.0112	1.157
BSF1208	4.263	1.180	4.050	0.8856	0.0015	0.5179	0.0179	1.403
BSF1307	5.047	1.335	4.602	0.9749	0.0007	0.8109	0.0370	1.785
BSF1406	2.585	1.740	2.551	1.7368	0.0045	0.0966	0.0368	1.833
BSF1505	4.118	1.929	4.075	1.6279	0.0014	0.4003	0.0278	2.028

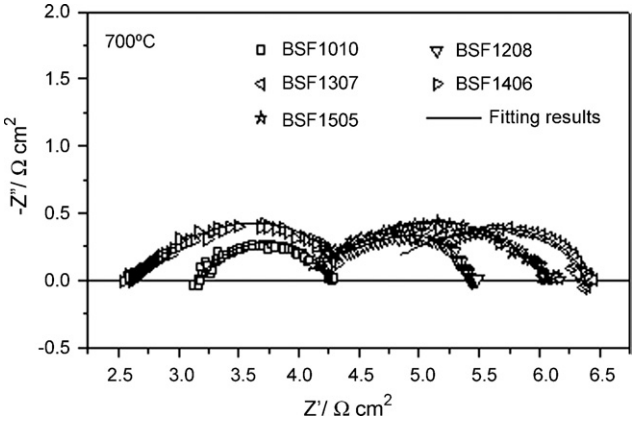

Fig. 8. Impedance spectra for $Ba_{2-x}Sr_xFeO_{4+\delta}$ (x = 0.5, 0.6, 0.7, 0.8, 1.0) cathodes at 700 °C under open-circuit-potential conditions.

gen adsorption or dissociation process [37]. The total polarization resistance (R_p) is the sum of R_1 and R_2. For the $Ba_{2-x}Sr_xFeO_{4+\delta}$ cathodes it can be seen from Table 1 that the high-frequency resistance is larger than that of the low-frequency, implying that O_2 reduction on the porous cathode is limited primarily by the charge-transfer process, presumably occurring at the TPB [38].

According to the impedance data obtained at different test temperatures, the temperature dependence of the polarization resistance for $Ba_{2-x}Sr_xFeO_{4+\delta}$ (x = 0.5, 0.6, 0.7, 0.8, 1.0) materials is plotted in Fig. 10. The apparent activation energy (E_a) calculated from the slope of the $\mathrm{Ln}(T/R_p)$ versus $1000/T$ plots is also included in Fig. 10. The polarization resistance decreased with the increase of the Sr doping content.

Fig. 11 shows the impedance spectra for a 48-h test of the BSF1010 cathode. There was only about 7% attenuation of the polarization resistance after the BSF1010 cathode was tested at 700 °C for 48 h, suggesting that the BSF1010 electrode was mechanically stable.

The cathode overpotential is an important factor representing the electrode performance [39]. The cathodic polarization curves for BSF1010 materials are plotted in Fig. 12. The lowest polarization overpotential of 0.064 V is measured for a BSF1010 cathode at

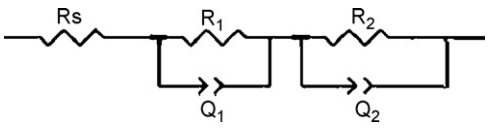

Fig. 9. Equivalent circuit used to fit the impedance data shown in Fig. 8.

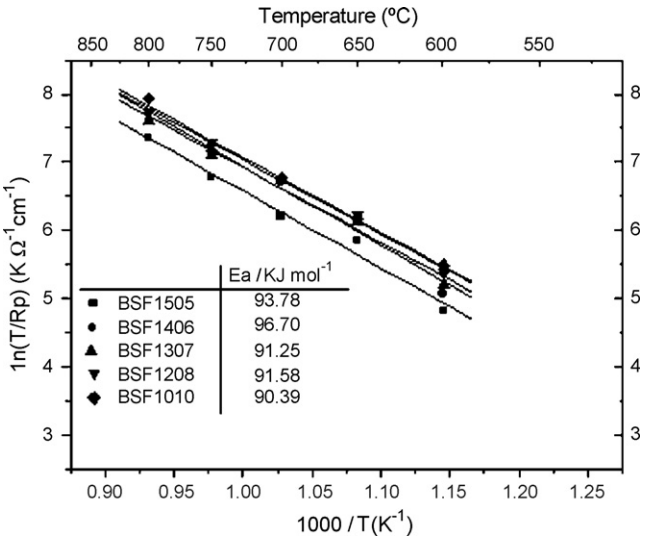

Fig. 10. Arrhenius plots of the polarization resistance for $Ba_{2-x}Sr_xFeO_{4+\delta}$ (x = 0.5, 0.6, 0.7, 0.8, 1.0) materials under open-circuit-potential conditions.

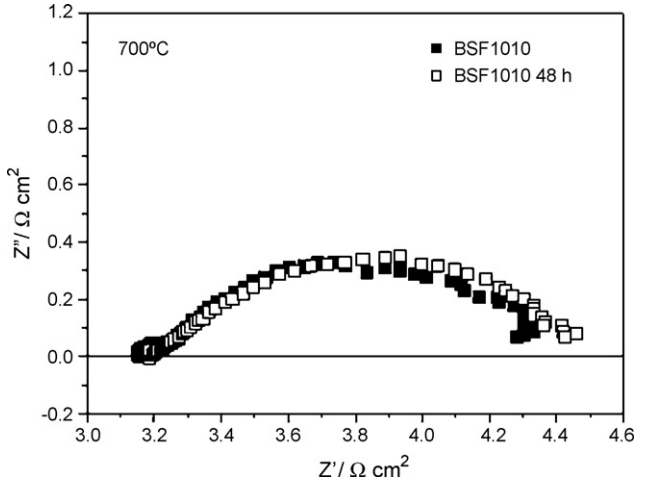

Fig. 11. Impedance spectra for a 48 h test of a BSF1010 cathode at 700 °C.

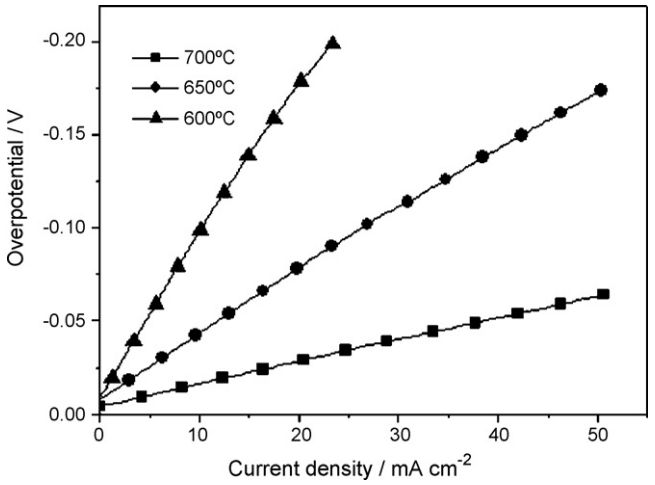

Fig. 12. Cathodic polarization curves for BSF1010 at different temperatures.

a current density of 51 mA cm^{-2} at 700 °C. Moreover, at low current density there appears to be a linear relationship [40], $i = i_0 ZF\eta/RT$, where i is the current density, i_0 is the exchange-current density, η is the overpotential, F is the Faraday constant and R is the universal gas constant. From the inverse of the derivative of i against η, the polarization resistance can be calculated. The value obtained at 700 °C is 1.25 Ω cm^2, which is in agreement with the result obtained from the impedance measurement.

4. Conclusions

$Ba_{2-x}Sr_xFeO_{4+\delta}$ (x = 0.5, 0.6, 0.7, 0.8, 1.0) materials were prepared and their potential as cathode materials for IT-SOFCs was evaluated. The electrochemical impedance spectra revealed that $Ba_{2-x}Sr_xFeO_{4+\delta}$ materials had a better electrochemical performance than Ln_2NiO_4 (Ln = La, Pr, Nd, Sm) materials. In the $Ba_{2-x}Sr_xFeO_{4+\delta}$ (x = 0.5, 0.6, 0.7, 0.8, 1.0) family, the composition $Ba_{1.0}Sr_{1.0}FeO_{4+\delta}$ showed the best electrochemical activity, especially for oxygen reduction. The polarization resistance of $Ba_{1.0}Sr_{1.0}FeO_{4+\delta}$ was 1.11 Ω cm^2 at 700 °C, nearly half that reported for Ln_2NiO_4 materials at the same temperature. TG results showed that there was more interstitial oxygen in $A_2BO_{4+\delta}$ materials after the bigger-radius Ba^{2+} replaced the smaller-radius Ln^{3+} (Ln = La, Pr, Nd, Sm). More oxygen overstoichiometry (δ) resulted in better electrochemical properties. According to the cathodic polarization results, the $Ba_{1.0}Sr_{1.0}FeO_{4+\delta}$ cathode exhibited a cathodic overpotential lower than 0.064 V at 700 °C at a current density of 51 mA cm^{-2}. The present experimental results suggest that $Ba_{1.0}Sr_{1.0}FeO_{4+\delta}$ is a potential cathode material for use in IT-SOFC.

Acknowledgements

The authors gratefully acknowledge financial support from the National Hi-tech 863 project of China (2007AA05Z136), the Department of Science and Technology of Guangdong Province (2005B50101007) and the Department of Education of Guangdong Province (B15N9060210).

References

[1] S.M. Haile, Acta Mater. 51 (2003) 5981–6000.
[2] J. Larminie, A. Dicks, Fuel Cell System Explained, John Wiley & Sons, Ltd., Chichester, 2000, p. 44.
[3] J. Fleig, J. Maier, J. Eur. Ceram. Soc. 24 (2004) 1343–1347.
[4] S.B. Adler, Chem. Rev. 104 (2004) 4791–4844.
[5] S.J. Skinner, Solid State Sci. 5 (2003) 419–426.
[6] V.V. Vashook, I.I. Yushkevich, L.V. Kokhanovsky, L.V. Makhnach, I.F. Kononyuk, H. Ullmann, H. Altenburg, Solid State Ionics 119 (1999) 23–30.
[7] S.J. Skinner, J.A. Kilner, Solid State Ionics 135 (2000) 709–712.
[8] V.V. Kharton, A.P. Viskup, A.V. Kovalesky, E.N. Naumovich, F.M.B. Marques, Solid State Ionics 143 (2001) 337–353.
[9] S.C. Chen, K.V. Ramanujachary, M. Greenblatt, J. Solid State Chem. 105 (1993) 444–457.
[10] M.A. Daroukh, V.V. Vashook, H. Ullmann, F. Tietzb, I. Arual Raj, Solid State Ionics 158 (2003) 141–150.
[11] Y.S. Wang, H.W. Nie, S.R. Wang, T.L. Wen, U. Guth, V. Valshook, Mater. Lett. 60 (2006) 1174–1178.
[12] E. Boehm, J.M. Bassat, M.C. Steil, P. Dordor, F. Mauvy, J.C. Grenier, Solid State Sci. 5 (2003) 973–981.
[13] E. Boehm, J.M. Bassat, P. Dordor, F. Mauvy, J.C. Grenier, Ph. Stevens, Solid State Ionics 176 (2005) 2717–2725.
[14] N. Solak, M. Zinkevich, F. Aldinger, Solid State Ionics 177 (2006) 2139–2142.
[15] M.L. Fontaine, C. Laberty-Robert, F. Ansart, P. Tailhades, J. Power Sources 156 (2006) 33–38.
[16] V. Vashook, J. Zosel, T.L. Wen, U. Guth, Solid State Ionics 177 (2006) 1827–1830.
[17] F. Mauvy, J.M. Bassat, E. Boehm, J.P. Manaud, P. Dordor, J.C. Grenier, Solid State Ionics 158 (2003) 17–28.
[18] C. Lalanne, F. Mauvy, E. Siebert, M.L. Fontaine, J.M. Bassat, F. Ansart, P. Stevens, J.C. Grenier, J. Eur. Ceram. Soc. 27 (2007) 4195–4198.
[19] Q. Li, Y. Fan, H. Zhao, L.P. Sun, L.H. Huo, J. Power Sources 167 (2007) 64–68.
[20] A.J. Jennings, S.J. Skinner, Solid State Ionics 152–153 (2000) 663–667.

[21] T. Omata, K. Ueda, N. Ueda, M. Katada, S. Fujitsu, T. Hashimoto, H. Kawazoe, Solid State Commun. 88 (1993) 807.
[22] V.V. Vashook, S.P. Tolochko, I.I. Yushkevich, L.V. Makhnach, I.F. Kononyuk, H. Altenburg, J. Hauck, H. Ullrnann, Solid State Ionics 110 (1998) 245–253.
[23] K. Ishikawa, S. Kondo, H. Okanc, S. Suzuki, Y. Suzuki, Bull. Chem. Soc. Jpn. 60 (1987) 1295–1298.
[24] L.A. Chick, L.R. Pederson, G.D. Maupin, J.L. Bates, L.E. Thomas, G.J. Exarhos, Mater. Lett. 10 (1990) 6–12.
[25] D.H.A. Blank, H. Kruidhof, J. Flokstra, J. Phys. D: Appl. Phys. 21 (1988) 226–232.
[26] D.C. Zhu, X.Y. Xu, S.J. Feng, W. Liu, C.S. Chen, Catal. Today 82 (2003) 151–156.
[27] C. Li, T.H. Hu, H. Zhang, Y. Chen, J. Jin, N.R. Yang, J. Membr. Sci. 226 (2003) 1–7.
[28] J.W.J. Potts, Chemical Infrared Spectroscopy, vol. 1, John Wiley & Sons Inc., New York, 1963, pp. 135–146.
[29] E.N. Naumovich, M.V. Patrakeev, V.V. Kharton, A.A. Yaremchenko, D.I. Logvinovich, F.M.B. Marques, Solid State Sci. 7 (2005) 1353–1362.
[30] V.V. Kharton, A.A. Yaremchenko, E.N. Naumovich, J. Solid State Electrochem. 3 (1999) 303–326.
[31] L. Minervini, R.W. Grimes, J.A. Kilner, K.E. Sickafus, J.C. Grenier, Ph. Stevens, J. Mater. Chem. 10 (2000) 2349–2354.
[32] J.M. Bassat, P. Odier, A. Villesuzane, C. Marin, M. Pouchard, Solid State Ionics 167 (2005) 52–56.
[33] A. Aguadero, J.A. Alonso, M.T. Fernandez-Dıaz, M.J. Escudero, L. Daza, J. Power Sources 169 (2007) 17–24.
[34] H. Zhang, J. Jin, G.Y. Yu, N.R. Yang, Chin. J. Inorg. Chem. 16 (2000) 911–915.
[35] H. Zhao, L.H. Huo, L.P. Sun, L.J. Yu, S. Gao, J.G. Zhao, Mater. Chem. Phys. 88 (2004) 160–166.
[36] Q. Li, Y. Fan, H. Zhao, L.H. Huo, Chin. J. Inorg. Chem. 22 (2006) 2025–2030.
[37] C.J. Fu, K.N. Sun, N.Q. Zhang, X.B. Chen, D.R. Zhou, Electrochim. Acta 52 (2007) 4589–4594.
[38] S.B. Adler, Solid State Ionics 111 (1998) 125–134.
[39] X.Q. Huang, J. Liu, Z. Lv, W. Liu, L. Pei, T.M. He, Z.G. Liu, W.H. Su, Solid State Ionics 130 (2000) 195–201.
[40] B.C.H. Steele, Solid State Ionics 75 (1995) 157–165.